Capping protein regulates actin dynamics during cytokinetic midbody maturation

Stephen J. Terry[a], Federico Donà[a], Paul Osenberg[b], Jeremy G. Carlton[b,c], and Ulrike S. Eggert[a,d,1]

[a]Randall Centre for Cell and Molecular Biophysics, School of Basic and Medical Biosciences, King's College London, SE1 1UL London, United Kingdom; [b]School of Cancer and Pharmaceutical Sciences, King's College London, SE1 1UL London, United Kingdom; [c]The Francis Crick Institute, NW1 1AT London, United Kingdom; and [d]Department of Chemistry, King's College London, SE1 1UL London, United Kingdom

Edited by Thomas D. Pollard, Yale University, New Haven, CT, and approved January 16, 2018 (received for review December 27, 2017)

During cytokinesis, a cleavage furrow generated by actomyosin ring contraction is restructured into the midbody, a platform for the assembly of the abscission machinery that controls the final separation of daughter cells. The polymerization state of F-actin is important during assembly, ingression, disassembly, and closure of the contractile ring and for the cytoskeletal remodeling that accompanies midbody formation and progression to abscission. Actin filaments must be cleared from the abscission sites before the final cut can take place. Although many conserved proteins interact with and influence the polymerization state of actin filaments, it is poorly understood how they regulate cytokinesis in higher eukaryotes. We report here that the actin capping protein (CP), a barbed end actin binding protein, participates in the control of actin polymerization during later stages of cytokinesis in human cells. Cells depleted of CP furrow and form early midbodies, but they fail cytokinesis. Appropriate recruitment of the ESCRT-III abscission machinery to the midbody is impaired, preventing the cell from progressing to the abscission stage. To generate actin filaments of optimal length, different actin nucleators, such as formins, balance CP's activity. Loss of actin capping activity leads to excessive accumulation of formin-based linear actin filaments. Depletion of the formin FHOD1 results in partial rescue of CP-induced cytokinesis failure, suggesting that it can antagonize CP activity during midbody maturation. Our work suggests that the actin cytoskeleton is remodeled in a stepwise manner during cytokinesis, with different regulators at different stages required for successful progression to abscission.

cytokinesis | capping protein | formins | midbody | F-actin

During cytokinesis, actomyosin ring contraction remodels the cellular cortex to generate a cleavage furrow and then, the midbody, a platform for the assembly of the abscission machinery that controls the final separation of daughter cells (1, 2). Although the overall progression of cytokinesis is well-documented, many questions remain, especially at the molecular level (3), in part due to the high spatial and temporal complexity of cytokinesis coupled to the requirement for significant force generation during cleavage. While the chromosomes separate during anaphase, a contractile ring assembles that includes actin, myosin, and many other proteins. The ring then ingresses, with actomyosin-based contraction providing the required mechanical force (4). Contractile ring assembly, ingression, and closure are regulated in part by Rho GTPase signaling, which triggers the activation of myosin and the formation of formin-based linear actin filaments (5, 6). As the ring ingresses and its diameter decreases, actin filaments must disassemble to allow complete ingression and subsequent formation of the midbody (7, 8). Much of our knowledge of the early steps of actin dynamics during cytokinesis has come from studies in model systems, such as fission yeast, because they are broadly conserved. More recently, it has become clear that the polymerization state of F-actin is also important postfurrowing, including during progression to abscission, events specific to higher eukaryotes. New and unexpected roles have been suggested for actin remodeling in the intercellular bridge during the last steps of cytokinesis, just before abscission (9–11).

The dynamic polymerization state of actin, regulated by many conserved proteins, is key to its many cellular functions. Actin nucleating proteins are required for actin filament assembly. For example, Arp2/3 promotes actin nucleation and generates short branched networks (6), but it does not seem to be a major regulator of metazoan cytokinesis. Formins nucleate and elongate linear actin filaments (6), and the formins cdc12, Diaphanous, and CYK-1 are important during contractile ring assembly in fission yeast, flies, and worms, respectively (12–14). While it is generally thought that formins are needed during mammalian cytokinesis (5), it is less clear which individual formins are required. So far, only mDia2/Diaph3 in mouse cells has been shown to be directly involved (15). To balance promotion of actin polymerization, proteins that sever and turnover actin filaments, such as ADF/Cofilin, also play important roles in cytokinesis (2). We report here that the actin capping protein (CP), a barbed end actin binding protein complex (16), is required to control actin polymerization during later stages of cytokinesis in human cells.

Results

CP Is Required for Cytokinesis in Human Cultured Cells. Knockdown of CP, a heteromeric protein complex consisting of α (CAPZA) and β (CAPZB) subunits (16), resulted in the formation of binucleated cells, a hallmark of failed cytokinesis (Fig. 1 *A–C* and Fig. S1 *A–C*). Failure could be rescued by stable expression of RNAi-resistant GFP-CAPZB (GFP-CAPZB^{R}) (Fig. S1 *D–G*) in two human cell lines representative of normal [human corneal epithelial (HCE) (17)] and cancerous (HeLa) tissues. Notably,

Significance

Actin dynamics drive many steps of cell division. Here, we show that the actin capping protein (CP) is unexpectedly involved in midbody maturation, a poorly understood phase of the cell cycle where cells remodel their intercellular bridges to prepare for separation. The loss of CP results in excessive filamentous actin throughout the cell cycle, but only postfurrowing cytokinesis is inhibited. We propose that optimal actin filament function is achieved by a balance between CP-dependent filament capping and formin-driven polymerization. This raises the intriguing possibility that cells utilize specific types of actin filament networks to progress through division. This finding has profound implications on understanding actin-dependent processes such as cell division, migration, adhesion, and morphogenesis.

Author contributions: S.J.T., F.D., J.G.C., and U.S.E. designed research; S.J.T., F.D., P.O., and J.G.C. performed research; S.J.T., F.D., J.G.C., and U.S.E. analyzed data; and S.J.T. and U.S.E. wrote the paper.

The authors declare no conflict of interest.

This article is a PNAS Direct Submission.

[1]To whom correspondence should be addressed. Email: ulrike.eggert@kcl.ac.uk.

This article contains supporting information online at www.pnas.org/lookup/suppl/doi:10.1073/pnas.1722281115/-/DCSupplemental.

Published online February 8, 2018.

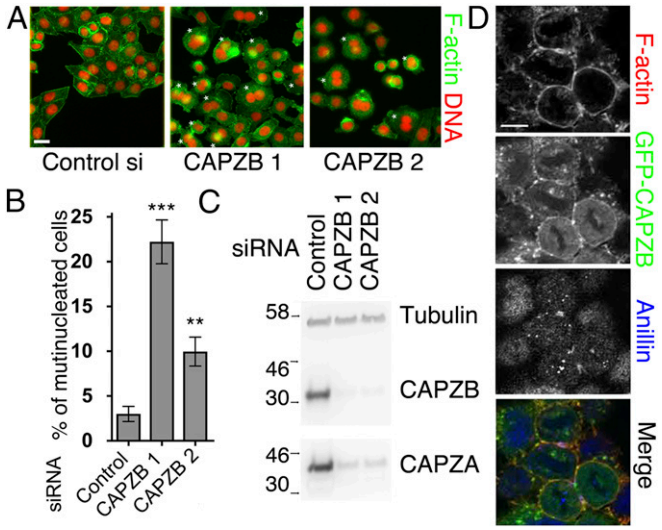

Fig. 1. CP is required for cytokinesis in human cells. (*A*) Representative epifluorescence images of HeLa cells fixed and stained with TRITC-phalloidin (green) and DAPI (red) to visualize F-actin and DNA, respectively, 72 h after siRNA transfection with either nontargeting control siRNA or two independent siRNA oligos for CAPZB (oligos 1 and 2). *Bi- or multinucleated cells. (Scale bar: 20 μm.) (*B*) Quantification of *A*. Data are presented as mean ± SD ($n = 3$); >300 cells were scored per experiment. $^{**}P < 0.01$; $^{***}P < 0.001$. (*C*) Immunoblot showing protein levels of CAPZA, CAPZB, and tubulin for cells from *B*. Note the expected destabilization of CAPZA in CAPZB-depleted cells. (*D*) Representative images from confocal sections of cytokinetic HeLa cells expressing GFP-CAPZB. Cells were fixed and stained with TRITC-phalloidin to visualize F-actin (red), anti-GFP (green), and anti-Anillin (blue). (Scale bar: 10 μm.)

GFP-CAPZB^{R} restored normal levels of CAPZA, indicating that it forms a functional dimer with the α subunit (Fig. S1 *F* and *G*). Codepletion of both α isoforms also resulted in a significant increase in multinucleated cells (Fig. S1 *H* and *I*), indicating that the entire CP complex is essential for cytokinesis.

CP Localizes to Cortical F-Actin Structures Throughout the Cell Cycle. During interphase, GFP-CAPZB localizes to cytoplasmic puncta and colocalizes with F-actin at the cortex and in lamellipodia-like structures (Fig. S1*J*) (18). Cytochalasin D treatment disrupted localization of GFP-CAPZB to both cortical actin structures and cytoplasmic puncta (Fig. S1*J*), indicating that its localization is dependent on a functional actin cytoskeleton. In dividing cells, GFP-CAPZB colocalized with F-actin at the cell cortex, the cleavage furrow, and the ingressed furrow surrounding the midbody (Fig. 1*D* and Fig. S1*K*), suggesting that it may function in control of cytoskeletal remodeling during division.

CP-Depleted Cells Complete Furrowing with Slow Kinetics. Using fluorescence time-lapse microscopy of dividing cells starting at 48 h post-RNAi, when CP is mostly depleted (Fig. S2 *A*–*D* and Movies S1 and S2), we found that CP-depleted cells placed their cleavage furrows correctly after progressing through mitosis (nuclear envelope breakdown to anaphase onset) with a delay (19) (Fig. 2*A* and Fig. S2*E*). We measured furrow ingression kinetics using GFP-tubulin, as interzonal microtubules are just below the contractile ring and are compacted to form the intercellular bridge. We compared control cells, CP-depleted cells, and cells where actin filaments were stabilized using a low dose (100 nM) of the actin-stabilizing compound jasplakinolide (higher doses prevent contractile ring formation). After anaphase onset, initial ingression was rapid in all three conditions (Fig. 2*B*), with the diameter of microtubule structures decreasing by around one-half to 11 μm within 8 min for control, 11 min for jasplakinolide-treated, and 12 min for CP-depleted cells (Fig. 2*B*). Control cells and jasplakinolide-treated cells then continued to ingress with similarly shaped ingression curves, although slower for jasplakinolide-treated cells, and slowed after reaching a diameter of around 4 μm, after which they further compacted their microtubules and formed midbodies. In contrast, CP-depleted cells slowed substantially after the halfway point

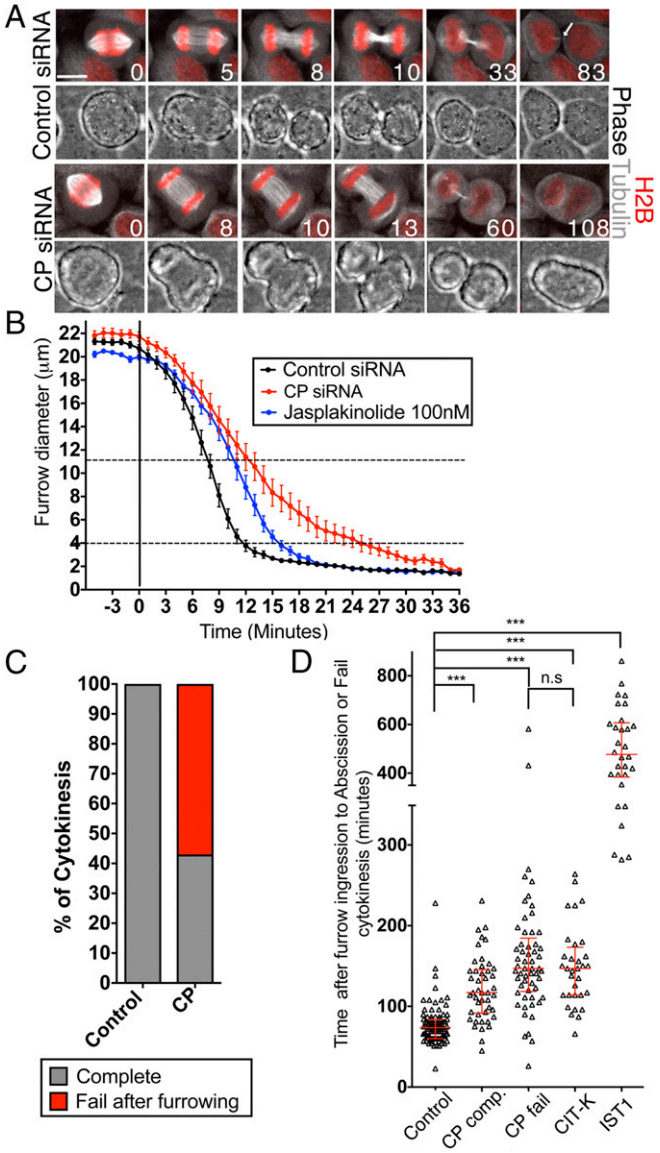

Fig. 2. CP-depleted cells fail cytokinesis postfurrowing. (*A*) Still images from confocal time-lapse movies of siRNA-transfected HeLa cells stably expressing GFP-tubulin (gray) and Histone2B-mCherry (red) shown as merged or phase contrast images. Time between frames is indicated in minutes, and timings are normalized to anaphase onset. White arrow indicates point of abscission. (Scale bar: 10 μm.) (*B*) Quantification of furrowing kinetics obtained by measuring furrow diameter at anaphase onset $t = 0$ using GFP-tubulin signal against time in minutes for cells treated with control siRNA ($n = 20$ cells) or CP siRNA ($n = 16$ cells) or treated before anaphase onset with 100 nM jasplakinolide ($n = 10$ cells). Data are from three independent experiments, and lines represent mean average. Error bars = SEM (Movies S1 and S2). (*C*) Quantification of percentage of HeLa cells failing cytokinesis after 50 h CP siRNA; 56% of cells fail postfurrowing vs. 0% for control. Control ($n = 90$) and CP siRNA ($n = 102$ cells) from three independent experiments are shown. (*D*) Scatterplot of time in minutes taken to progress from after furrow ingression to abscission of indicated siRNA treatments. Red bars represent medians and upper and lower quartiles (Movies S3 and S4). n.s., not significant ($P > 0.05$). $^{***}P < 0.001$.

(Fig. 2*B*). The differences in ingression kinetics of CP-depleted and jasplakinolide-treated cells suggest that the phenotype induced by CP depletion is not due to generic stabilization of actin filaments and may stem from an inability to properly regulate filament length within the forming midbody.

CP-Depleted Cells Fail Cytokinesis After Furrowing. While cells lacking CP ingress more slowly, they eventually complete furrowing. Time-lapse analysis revealed that cytokinesis predominantly fails postfurrowing (Fig. 2 *C* and *D* and Movies S1 and S2). CP-depleted HeLa cells undergo cleavage furrow regression within a median of 147 min (median to completion in control cells = 73.5 min). Cells depleted of CIT-K, a kinase necessary for midbody maturation (20), fail cytokinesis with similar kinetics to CP with a median of 147 min (Fig. 2*D*, Fig. S2 *F* and *G*, and Movies S3 and S4). In contrast, depletion of the ESCRT-III component IST1 (21, 22) results in cytokinesis failure after prolonged abscission arrest, with a median of 477 min (Fig. 2*D*, Fig. S2 *F* and *G*, and Movie S4). Consistent with this, while CP depletion induced cytokinesis failure, we failed to observe an accumulation of cells with visible intercellular bridges (Fig. S2*H*), suggesting that cytokinesis failure occurs before abscission. These data suggest that CP, like CIT-K, functions in midbody maturation rather than abscission.

CP-Depleted Cells Organize a Functional Midzone and Form a Midbody. Consistent with our live imaging results showing that CP-depleted cells fail cytokinesis after furrow ingression, anaphase midzones in CP-depleted cells appeared normal (Fig. S3*A*). CIT-K was properly recruited to the cleavage furrow and midbody (Fig. S3*B*). Similarly, depleted cells could recruit the centralspindlin complex (RacGAP1 and MKLP1) to the midbody ring and the Aurora B kinase to midbody flanking microtubules (Fig. S3*B*); thus, cytokinesis failure does not result from a failure to recruit these proteins.

CP-Dependent Control of F-Actin Levels Is Required for Its Role in Cytokinesis. Measuring global F-actin levels by flow cytometry in asynchronous populations of cells revealed that CP-depleted cells have 1.8-fold more F-actin than control cells (Fig. S4 *A* and *B*). A similar 1.8-fold increase relative to control in CP-depleted interphase HeLa cells (Fig. 3*A* and Fig. S4 *C*–*G*) increased to 2.4-fold in cytokinetic cells and 4.2-fold at the cleavage furrow (Fig. 3*B* and Fig. S4 *F* and *G*). Superresolution microscopy showed that the actin ultrastructure in early bridges differs between CP-depleted and control cells, with denser and more compacted actin structures in CP-depleted cells (Fig. 3*C* and Movies S5 and S6). These data suggest that excessive actin polymerization in the absence of CP interferes with proper completion of cytokinesis.

As CP may be involved in mitosis independent of its capping function (19), we tested if its role in cytokinesis was related to its ability to influence actin polymerization. We generated stable cell lines expressing GFP-CAPZB^R or GFP-CAPZB^R L262S mutant, which cannot bind the barbed end of growing actin filaments (23). The mutant protein could form a functional dimer as seen by the restoration of levels of CAPZA (Fig. S5*A*). However, in the absence of endogenous CAPZB, the L262S mutant failed to support cytokinesis (Fig. 3 *D* and *E*), showing that CP-dependent regulation of F-actin capping is necessary for cytokinesis.

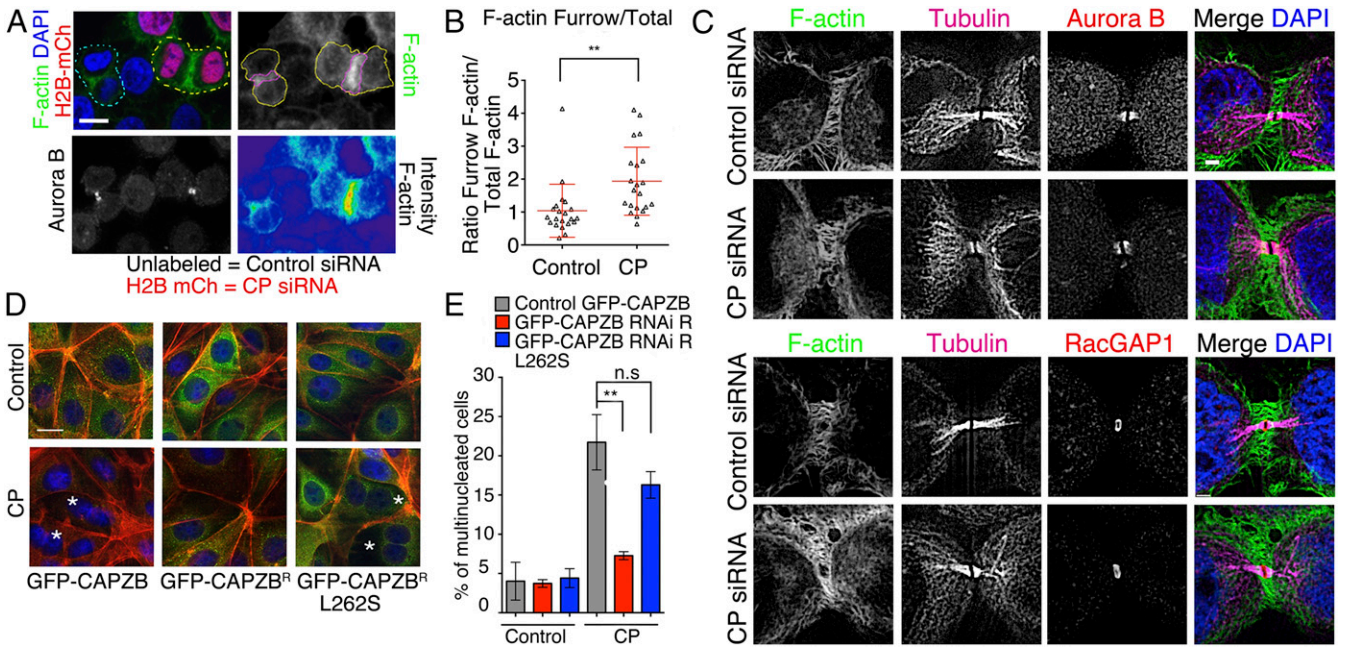

Fig. 3. CP-dependent control of F-actin levels is required for cytokinesis. (*A*) Representative confocal images of cytokinetic HeLa cells. Unlabeled cells were treated with control siRNA and mixed with H2B-mCherry–labeled cells transfected with CAPZB siRNA. Cells were fixed 72 h after RNAi transfection (Fig. S4). Merged images of cells stained with FITC-phalloidin to visualize F-actin (green), H2B-mCherry (red), and DAPI (blue) are shown. Dashed yellow and cyan lines mark outlines of CAPZB-depleted and control-treated cells, respectively. Immunostaining with Aurora B (gray; *Lower*) was used to define comparable stages of cytokinesis. FITC-phalloidin (gray; *Upper*) was used for total and furrow F-actin quantifications shown in *B*. Yellow and pink outlines in *Upper Right* represent regions of interest. *Lower* is the intensity of F-actin in pseudocolor. (Scale bar: 10 μm.) (*B*) Graph showing ratio of furrow F-actin vs. total F-actin for cytokinetic control or CAPZB siRNA-transfected cells (n = 20 cells per condition) collected from two independent experiments. Red bars represent medians and upper and lower quartiles; the numbers discussed in the text are medians. $^{**}P < 0.001$. (*C*) Representative 3D SIM reconstructions of cytokinetic cells of siRNA-transfected cells stained with FITC-phalloidin to visualize F-actin (green), tubulin (magenta), Aurora B or RacGAP1 (red), and DAPI (blue). Images are presented as maximum intensity projections of 1- to 0.5-μm z sections (representative of 10 images per siRNA treatment). Note that SIM does not report on intensity. Movies S5 and S6 show full reconstructions of z series. (Scale bar: 2 μm.) (*D*) Representative confocal images of siRNA-transfected HCE cells expressing GFP-CAPZB, GFP-CAPZB^R, and GFP-CAPZB^R L262S immunostained with anti-GFP (green), TRITC-phalloidin (red) to visualize F-actin, and DAPI (blue). *Multinucleated cells. (Scale bar: 20 μm.) (*E*) Graph showing level of multinucleation in HCE cells transfected with control or CP siRNA and stably expressing GFP-CAPZB, GFP-CAPZB^R, or GFP-CAPZB^R L262S. Data are presented as mean ± SD (n = 3) from n > 200 cells per experiment. n.s., not significant ($P > 0.05$). $^{**}P < 0.001$.

CP-Depleted Cells Form Midbodies with Incorrectly Recruited ESCRT-III. The midbody acts as a platform for the recruitment of the abscission machinery, where CEP55 at the midbody ring forms a scaffold for the recruitment of ESCRT proteins (24, 25). In fixed cells, midbody-flanking microtubules in CP-depleted cells were thicker than in control (Fig. 4 *A* and *B*). To determine if thicker intercellular bridges were due to a failure to fully compact or due to complete ingression followed by relaxation, we used live imaging in CEP55-GFP cells treated with SiR-tubulin, a microtubule dye. With measurement beginning 1 h before abscission or failure, we found that midbody rings in CP-depleted cells never reached full compaction and that CP-depleted cells that failed cytokinesis had thicker CEP55-positive midbody rings than cells that eventually divided (Fig. 4 *C* and *D* and Movie S7). These data suggest that capping of actin filaments is necessary for normal thinning of the midbody, an important prerequisite for abscission.

After the microtubules of the intercellular bridge have compacted sufficiently and the midbody has begun to assemble ("early midbody"), ESCRT-III subunits are recruited to two rings adjacent to the midbody ring ("maturing midbody") (Fig. 4 *E–G* and Movies S8 and S9) (26, 27). Immediately before abscission, a pool of ESCRT-III relocates to secondary ingression sites further along the intercellular bridge, where cleavage occurs (10, 27, 28). Formation of this secondary ingression is dependent on remodeling of the actin cytoskeleton in the midbody (10, 11). Interestingly, ESCRT-III was still recruited to midbodies in CP-depleted and control cells (Fig. 3*B*). However, ESCRT-III localization patterns were perturbed (Fig. 4 *E–G*). We staged ESCRT-III localization according to the work by Caballe et al. (29) and found that the absence of CP prevented proper formation of ESCRT-III assemblies at the two-ring stage, with a large proportion of cells displaying fragmented ESCRT-III structures instead (Fig. 4 *E–G*). These data suggest that, as well as regulating midbody dimensions/size, the correct polymerization state of actin is necessary for proper assembly of the abscission machinery.

Chemical Inhibition of Actin Polymerization Relieves the CP Depletion-Induced Cytokinesis Defect. If defective capping results in inappropriately elongated actin filaments responsible for cytokinesis failure, we wondered if normal division could be restored by artificially shortening actin filaments. Gross inhibition of actin polymerization using 500 nM Latrunculin B and Cytochalasin D resulted in robust cytokinesis failure (Fig. S6 *A* and *B*) (30). However, treatment with these compounds at concentrations that minimally disrupt cytokinesis (75 nM for Latrunculin B and 7.5 nM for Cytochalasin D) (Fig. 5*A*) relieved CP depletion-mediated cytokinesis failure, indicating that cytokinesis failure in CP-depleted cells occurs due to unchecked actin polymerization.

Actin polymerization is driven by different factors, including Arp2/3, which balances CP function in other cytoskeletal processes (6, 16). Consistent with a reported lack of Arp2/3 involvement in

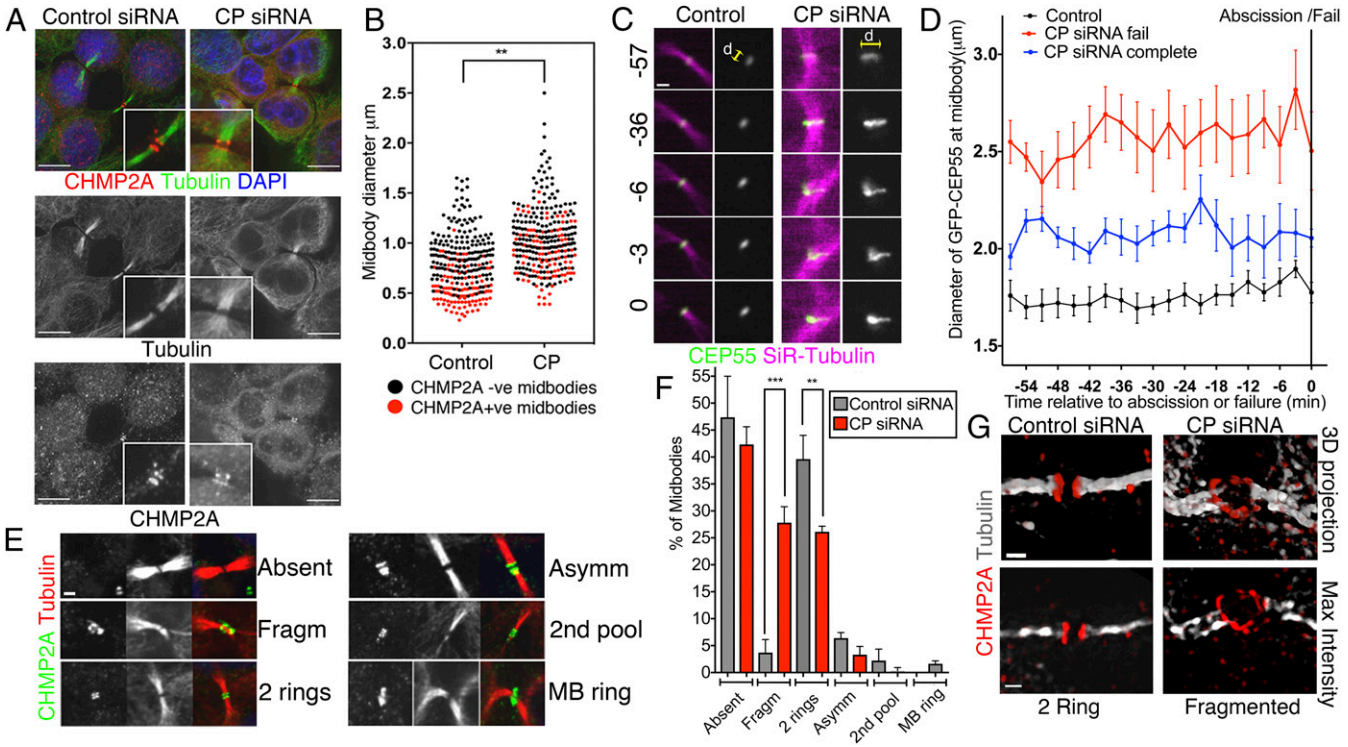

Fig. 4. CP-depleted cells display defects in midbody maturation. (*A*) Representative images of siRNA-transfected HeLa cells stained with tubulin (green), CHMP2A (red), and DAPI (blue). *Insets* show zoomed-in views of midbodies. (Scale bar: 10 µm.) (Magnification: *Insets*, 3.5×.) (*B*) Quantification of images from *A*; 288 cells were imaged from three independent experiments. Average midbody diameter: control siRNA, 0.78 ± 0.05 µm; CP siRNA, 1.04 ± 0.01 µm; mean ± SEM ($n = 3$). No significant difference in the percentage of midbodies that were CHMP2A-positive ($P = 0.87$). $^{**}P = 0.03$ (two-tailed *t* test). (*C*) Zoomed-in views of still images of midbodies from time-lapse movies of siRNA-transfected HeLa cells line stably expressing GFP-CEP55 (green/gray) and treated with SiR-tubulin (magenta) (Movie S7). Time in minutes is shown on the left adjusted to 57 min before abscission; d with the yellow bar indicates midbody ring diameter. (Scale bar: 2 µm.) (*D*) Quantification of images from *C* showing the diameter of GFP-CEP55 midbody ring signal prior to abscission or cytokinesis failure ($t = 0$). Control siRNA ($n = 10$), CP siRNA complete ($n = 8$), CP siRNA fail ($n = 6$). Bars represent mean ± SEM ($n = 2$). (*E*) Representative confocal images of midbodies from HeLa cells stained with tubulin (red) and CHMP2A (green). Shown are different categories of CHMP2A localization found in control and CP-depleted cells. (Scale bar: 2 µm.) (*F*) Quantification of *E* showing percentages of midbodies displaying different localization categories of CHMP2A recruitment. Bars represent means, and error bars = SD ($n = 3$) counting >200 midbodies per experiment. $^{**}P = 0.007$ (two-tailed *t* test); $^{***}P = 0.0004$ (two-tailed *t* test). (*G*) 3D and maximum intensity projections of the 3D SIM-reconstructed 4-µm *z* series showing tubulin (gray) and CHMP2A (red). Control image represents the two-ring stage, and CP image represents the fragmented phenotype, representative of 10 images per siRNA treatment. (Scale bar: 1 µm.) Movies S8 and S9 show the full 3D reconstructions. MB, midbody.

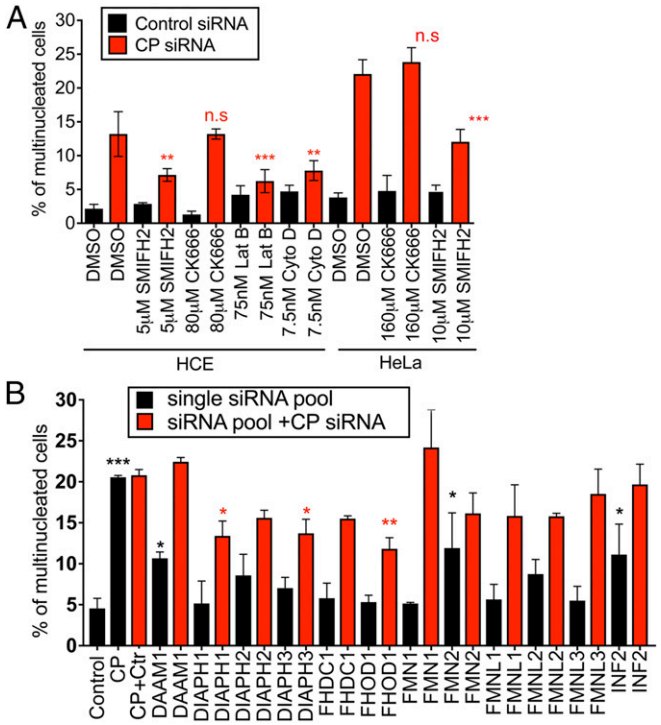

Fig. 5. Chemical inhibition of actin polymerization and RNAi depletion of individual formins potentiate CP depletion-induced cytokinesis failure. (*A*) Graph showing level of multinucleation in HeLa and HCE cells transfected with control or CP siRNA after treatment with control DMSO, pan formin inhibitor SMIFH2, Arp2/3 inhibitor CK666, or actin depolymerizing compounds Latrunculin B (Lat B) or Cytochalasin D (Cyto D). Data are presented as mean ± SD ($n = 3$) from $n > 200$ cells per experiment. n.s., not significant ($P > 0.05$) compared with CP DMSO treatment using one-way ANOVA using uncorrected Fisher's LSD test compared with CP siRNA. $^{**}P < 0.001$; $^{***}P < 0.0001$. (*B*) Graph showing percentage of multinucleated HeLa cells after transfection with control nontargeting siRNA, CP siRNA, and siRNA pools targeting the 12 formin proteins known to be expressed in HeLa cells. Percentage of multinucleated cells transfected with control nontargeting, CP or single formin siRNA (black bars) or formin siRNA pools + CP siRNA (red bars). Data are presented as mean ± SD ($n = 2$); $n > 300$ cells per treatment. Black asterisks indicate significance compared with control siRNA using one-way ANOVA using uncorrected Fisher's LSD test ($^{*}P < 0.01$; $^{***}P < 0.0001$). Red asterisks indicate significance compared with control + CP siRNA using one-way ANOVA using uncorrected Fisher's LSD test ($^{*}P < 0.01$; $^{**}P < 0.001$). LSD, least significant difference.

cytokinesis, inhibition of Arp2/3 function by treatment with the small molecule inhibitor CK666 (31) or Arp3 siRNA did not rescue CP-dependent cytokinesis failure (Fig. 5*A* and Fig. S6 *C–F*), although the overall actin cytoskeleton changed as expected (Fig. S6*C*). Formins elongate linear actin filaments and are important during contractile ring assembly in model organisms (6, 12–14). CP and formins both bind to the barbed end and have opposing roles in actin polymerization in vitro (32) and in *Schizosaccharomyces pombe* (33). However, due to functional redundancy of formins in mammalian cells, no specific formin has been implicated in human cytokinesis. We, therefore, used the pan formin inhibitor SMIFH2 to inhibit formin activity (34, 35) and found that 5 μM SMIFH2 partially rescues cytokinesis failure in CP-depleted cells (Fig. 5*A* and Fig. S6 *G–I*). Taken together, these data suggest an essential functional requirement of CP during cytokinesis to negatively regulate cortical F-actin polymerization by counteracting formin activity.

RNAi Depletion of Individual Formins Potentiates CP Depletion-Induced Cytokinesis Failure. We next determined if any specific formins might balance actin capping during cytokinesis; 12 of 15 human formins with partly overlapping functions are reportedly expressed in HeLa (36, 37). We screened a small RNAi library with these 12 formins for cytokinesis failure in the presence and absence of CP depletion. Consistent with the literature, depletion of none of the formins alone resulted in strong cytokinesis failure (Fig. 5*B* and Fig. S7). Depletion of the diaphanous formins (DIAPH1-3) (Fig. S7 *A* and *C*), thought to be the main actin nucleators in the contractile ring, partly rescued CP depletion. Intriguingly, depletion of the midbody-localized formin FHOD1 (38), however, rescued CP depletion more robustly (Fig. 5*B* and Fig. S7 *B* and *C*). It is possible that FHOD1, in conjunction with CP, is involved in creating actin filaments that are required to progress to midbody maturation.

Discussion

Cells accomplish different actin-dependent processes by using a variety of proteins, such as CP and formins, to regulate the polymerization state and architecture of the actin cytoskeleton. For example, a recent report analyzed the regulation of cell surface tension during mitosis (39). Cortical tension was reduced both in cells with shorter and thinner actin filaments (due to depletion of the formin DIAPH1) and in cells with longer and thicker filaments (due to CP depletion), suggesting that correct filament size is essential. Indeed, the interactions between formins and CP are variably regulated to achieve correct filament lengths (40). Individually, formins and CP bind to mutually exclusive binding sites at the barbed end, although ternary complexes have been reported where CP inhibits DIAPH1 and FMNL2 (40). We show here that CP, balanced by formins, is involved in cytokinesis in human cells. Our data hint at a carefully regulated network during cytokinesis that requires the right balance between actin polymerization and capping to achieve optimal filament length.

To ensure faithful maintenance of genetic and other cellular materials, dividing cells must precisely regulate a series of steps culminating in abscission. Although actin is a key participant in nearly all steps of cytokinesis, the detailed orientation of actin filaments in the ingressing furrow has only very recently been visualized (4). As the contractile ring ingresses rapidly, the diameter of the actin ring does not increase substantially, suggesting that actin is removed. Shortening of actin filaments (7, 41) as well as filament ejection due to changes in tension forces have been implicated in the disassembly during ingression (8), but molecular details have been elusive (3).

As the ring closes, the midbody is formed, with key proteins arriving sequentially and localizing to different areas within the intercellular bridge (42), followed by formation of abscission sites next to the midbody ring (Fig. 3*E*). Both actin and microtubule cytoskeletons have to be remodeled substantially and must be cleared from the secondary ingression sites to allow cleavage. It is largely unknown how the actin cytoskeleton is remodeled post-ingression, except for the very last step: different pathways mediated by Rab35 and FIP3 bring in factors that suppress actin polymerization (9, 10). In addition, MICAL1 actively induces actin depolymerization (11). When these late actin remodeling factors are perturbed, the ESCRT-III complex localizes correctly at the midbody but not at the secondary abscission sites, and cytokinesis is delayed for many hours. Interestingly, distinct but nonredundant pathways are needed for preabscission actin clearance, highlighting the importance of the correct execution of this step. For example, depletion of MICAL1 resulted in cytokinesis delays in a high percentage of cells, but only 4.1% fail outright (11). CP depletion causes 56% of actively dividing cells to fail postfurrowing, and many more are slowed but still eventually divide, suggesting that perhaps another redundant pathway also regulates this step of actin remodeling.

Our work identifies factors that regulate the polymerization state of actin before the formation of abscission sites. The requirement for further actin restructuring after the actin-rich ring has ingressed is conceptually straightforward and should logically be distinct from actomyosin disassembly during ingression, since the mechanical and regulatory environments that drive actin

turnover during ingression are no longer present. However, no such proteins had been identified. Given the complexity of disassembling and removing a structure as large and dense as the ingressed contractile ring, it would be plausible for the cell to do this in a stepwise manner. This could include a first step of shifting from DIAPH nucleated filaments to filaments regulated by CP and FHOD1 in early and maturing midbodies. While no functional analysis has been reported, FHOD1 was identified as a cytokinesis-specific Aurora B kinase interactor and was shown to localize to the midzone and midbody (38). It has been proposed that actin turnover in the constricting ring is due to shortening filaments (7, 41). One could speculate that CP/FHOD1 filaments are again shorter, which is supported by a recent report that FHOD1 is an unusual formin that prefers shorter filaments in some circumstances and does not act as a nucleator at all in others (43). Our superresolution images showing differences in the actin ultrastructure in early midbodies in CP vs. control cells (Fig. 3*C* and Movies S5 and S6) also tentatively support this model. Further remodeling culminating in complete clearance of actin from the abscission sites could then be initiated.

CP is connected to many different actin structures in cells, yet we show that CP-regulated filaments, likely balanced by FHOD1, are particularly important during postingression, preabscission cytokinesis. Our data also hint that CP may balance DIAPH formins during cytokinesis, although this seems less essential. The dynamic actin cytoskeleton is multifaceted and has been challenging to study in complex processes, such as cytokinesis, due to its ubiquity and involvement in many distinct yet overlapping steps. CP-dependent actin filaments illustrate this point; the overall F-actin in cells changes on CP depletion, and processes, such as contractile ring ingression, are moderately affected. However, the predominant phenotype in CP-depleted cells is postingression, raising the intriguing possibility that different networks of actin filaments with unique polymerization characteristics are required during different steps of cell division. This provides an intuitive explanation for how the same protein network can carry out a myriad of functions. Our data show that CP is a critical regulator of actin polymerization during midbody maturation. If actin is not in the correct polymerization state at this crucial stage, then cells cannot form mature midbodies and cannot divide.

Materials and Methods

For RNAi experiments, HeLa cells were transfected with siGENOME siRNAs (Dharmacon; GE Healthcare) using Interferin transfection reagent (Polyplus-Transfection Inc.). Samples for immunofluorescence and immunoblots were collected and processed 72 h after transfection, and for live cell imaging, they were collected and processed 50–72 h after transfection. For counts of multinucleated cells, mean and one SD from the mean were calculated for $n \geq 3$ independent experiments unless otherwise stated (typically >200 cells were counted for each data point experiment). A full list of siRNAs, antibodies, and reagents and detailed methods are described in *SI Materials and Methods*.

ACKNOWLEDGMENTS. We thank the Nikon Imaging Centre at King's College London for help with light microscopy, the Programme in Infection and Immunity Flow Cytometry Facility at King's College London for access to FACS technologies, and Elisabeth Ehler for FHOD1 antibodies. This work was funded by NIH Grant R01 GM082834, European Research Council Consolidator Grant 306659 (to U.S.E.), the European Molecular Biology Organization Young Investigator Programme (to J.G.C.), Wellcome Investigator Award 110060/Z/15/Z (to U.S.E.), and Wellcome Trust Fellowships 093603/Z/10/Z and 206346/Z/17/Z (to J.G.C.).

1. Mierzwa B, Gerlich DW (2014) Cytokinetic abscission: Molecular mechanisms and temporal control. *Dev Cell* 31:525–538.
2. Eggert US, Mitchison TJ, Field CM (2006) Animal cytokinesis: From parts list to mechanisms. *Annu Rev Biochem* 75:543–566.
3. Pollard TD (2017) Nine unanswered questions about cytokinesis. *J Cell Biol* 216: 3007–3016.
4. Spira F, et al. (2017) Cytokinesis in vertebrate cells initiates by contraction of an equatorial actomyosin network composed of randomly oriented filaments. *eLife* 6:e30867.
5. Bohnert KA, Willet AH, Kovar DR, Gould KL (2013) Formin-based control of the actin cytoskeleton during cytokinesis. *Biochem Soc Trans* 41:1750–1754.
6. Skau CT, Waterman CM (2015) Specification of architecture and function of actin structures by actin nucleation factors. *Annu Rev Biophys* 44:285–310.
7. Carvalho A, Desai A, Oegema K (2009) Structural memory in the contractile ring makes the duration of cytokinesis independent of cell size. *Cell* 137:926–937.
8. Huang J, et al. (2016) Curvature-induced expulsion of actomyosin bundles during cytokinetic ring contraction. *eLife* 5:e21383.
9. Dambournet D, et al. (2011) Rab35 GTPase and OCRL phosphatase remodel lipids and F-actin for successful cytokinesis. *Nat Cell Biol* 13:981–988.
10. Schiel JA, et al. (2012) FIP3-endosome-dependent formation of the secondary ingression mediates ESCRT-III recruitment during cytokinesis. *Nat Cell Biol* 14:1068–1078.
11. Frémont S, et al. (2017) Oxidation of F-actin controls the terminal steps of cytokinesis. *Nat Commun* 8:14528.
12. Chang F, Drubin D, Nurse P (1997) cdc12p, a protein required for cytokinesis in fission yeast, is a component of the cell division ring and interacts with profilin. *J Cell Biol* 137:169–182.
13. Castrillon DH, Wasserman SA (1994) Diaphanous is required for cytokinesis in Drosophila and shares domains of similarity with the products of the limb deformity gene. *Development* 120:3367–3377.
14. Swan KA, et al. (1998) cyk-1: A C. elegans FH gene required for a late step in embryonic cytokinesis. *J Cell Sci* 111:2017–2027.
15. Watanabe S, et al. (2010) Rho and anillin-dependent control of mDia2 localization and function in cytokinesis. *Mol Biol Cell* 21:3193–3204.
16. Edwards M, et al. (2014) Capping protein regulators fine-tune actin assembly dynamics. *Nat Rev Mol Cell Biol* 15:677–689.
17. Terry SJ, et al. (2011) Spatially restricted activation of RhoA signalling at epithelial junctions by p114RhoGEF drives junction formation and morphogenesis. *Nat Cell Biol* 13:159–166.
18. Schafer DA, et al. (1998) Visualization and molecular analysis of actin assembly in living cells. *J Cell Biol* 143:1919–1930.
19. di Pietro F, et al. (2017) An RNAi screen in a novel model of oriented divisions identifies the actin-capping protein Z β as an essential regulator of spindle orientation. *Curr Biol* 27:2452–2464.e8.
20. Bassi ZI, Audusseau M, Riparbelli MG, Callaini G, D'Avino PP (2013) Citron kinase controls a molecular network required for midbody formation in cytokinesis. *Proc Natl Acad Sci USA* 110:9782–9787.
21. Bajorek M, et al. (2009) Biochemical analyses of human IST1 and its function in cytokinesis. *Mol Biol Cell* 20:1360–1373.
22. Agromayor M, et al. (2009) Essential role of hIST1 in cytokinesis. *Mol Biol Cell* 20: 1374–1387.
23. Wear MA, Yamashita A, Kim K, Maéda Y, Cooper JA (2003) How capping protein binds the barbed end of the actin filament. *Curr Biol* 13:1531–1537.
24. Morita E, et al. (2007) Human ESCRT and ALIX proteins interact with proteins of the midbody and function in cytokinesis. *EMBO J* 26:4215–4227.
25. Carlton JG, Martin-Serrano J (2007) Parallels between cytokinesis and retroviral budding: A role for the ESCRT machinery. *Science* 316:1908–1912.
26. Carlton JG, Caballe A, Agromayor M, Kloc M, Martin-Serrano J (2012) ESCRT-III governs the Aurora B-mediated abscission checkpoint through CHMP4C. *Science* 336:220–225.
27. Elia N, Sougrat R, Spurlin TA, Hurley JH, Lippincott-Schwartz J (2011) Dynamics of endosomal sorting complex required for transport (ESCRT) machinery during cytokinesis and its role in abscission. *Proc Natl Acad Sci USA* 108:4846–4851.
28. Guizetti J, et al. (2011) Cortical constriction during abscission involves helices of ESCRT-III-dependent filaments. *Science* 331:1616–1620.
29. Caballe A, et al. (2015) ULK3 regulates cytokinetic abscission by phosphorylating ESCRT-III proteins. *eLife* 4:e06547.
30. Atilla-Gokcumen GE, Castoreno AB, Sasse S, Eggert US (2010) Making the cut: The chemical biology of cytokinesis. *ACS Chem Biol* 5:79–90.
31. Nolen BJ, et al. (2009) Characterization of two classes of small molecule inhibitors of Arp2/3 complex. *Nature* 460:1031–1034.
32. Bombardier JP, et al. (2015) Single-molecule visualization of a formin-capping protein 'decision complex' at the actin filament barbed end. *Nat Commun* 6:8707.
33. Kovar DR, Wu JQ, Pollard TD (2005) Profilin-mediated competition between capping protein and formin Cdc12p during cytokinesis in fission yeast. *Mol Biol Cell* 16:2313–2324.
34. Rizvi SA, et al. (2009) Identification and characterization of a small molecule inhibitor of formin-mediated actin assembly. *Chem Biol* 16:1158–1168.
35. Eggert US, Field CM, Mitchison TJ (2006) Small molecules in an RNAi world. *Mol Biosyst* 2:93–96.
36. Uhlen M, et al. (2017) A pathology atlas of the human cancer transcriptome. *Science* 357:eaan2507.
37. Krainer EC, et al. (2013) The multiplicity of human formins: Expression patterns in cells and tissues. *Cytoskeleton (Hoboken)* 70:424–438.
38. Ozlü N, et al. (2010) Binding partner switching on microtubules and aurora-B in the mitosis to cytokinesis transition. *Mol Cell Proteomics* 9:336–350.
39. Chugh P, et al. (2017) Actin cortex architecture regulates cell surface tension. *Nat Cell Biol* 19:689–697.
40. Shekhar S, et al. (2015) Formin and capping protein together embrace the actin filament in a ménage à trois. *Nat Commun* 6:8730.
41. Maupin P, Pollard TD (1986) Arrangement of actin filaments and myosin-like filaments in the contractile ring and of actin-like filaments in the mitotic spindle of dividing HeLa cells. *J Ultrastruct Mol Struct Res* 94:92–103.
42. Hu CK, Coughlin M, Mitchison TJ (2012) Midbody assembly and its regulation during cytokinesis. *Mol Biol Cell* 23:1024–1034.
43. Patel AA, Oztug Durer ZA, van Loon AP, Bremer KV, Quinlan ME (2018) Drosophila and human FHOD family formins nucleate actin filaments. *J Biol Chem* 293:532–540.